PHYSICAL REVIEW B **82**, 115202 (2010)

Mid-gap electronic states in $Zn_{1-x}Mn_xO$

Claire A. Johnson,[1] Kevin R. Kittilstved,[1] Tiffany C. Kaspar,[2] Tim C. Droubay,[2] Scott A. Chambers,[2] G. Mackay Salley,[1,3] and Daniel R. Gamelin[1,*]

[1]*Department of Chemistry, University of Washington, Seattle, Washington 98195-1700, USA*

[2]*Pacific Northwest National Laboratory, Richland, Washington 99352, USA*

[3]*Department of Physics, Wofford College, Spartanburg, South Carolina 29303, USA*

(Received 10 July 2010; published 2 September 2010)

Electronic absorption, magnetic circular dichroism (MCD), photoconductivity, and valence-band x-ray photoelectron (XPS) spectroscopic measurements were performed on epitaxial $Zn_{1-x}Mn_xO$ films to investigate the origin of the mid-gap band that appears upon introduction of Mn^{2+} into the ZnO lattice. Absorption and MCD spectroscopies reveal Mn^{2+}-related intensity at energies below the first excitonic transition of ZnO, tailing well into the visible energy region, with an onset at ~2.2 eV. Photoconductivity measurements show that excitation into this visible band generates mobile charge carriers, consistent with assignment as a $Mn^{2+/3+}$ photoionization transition. XPS measurements reveal the presence of occupied Mn^{2+} levels just above the valence-band edge, supporting this assignment. MCD measurements additionally show a change in sign and large increase in magnitude of the excitonic Zeeman splitting in $Zn_{1-x}Mn_xO$ relative to ZnO, suggesting that *sp-d* exchange in $Zn_{1-x}Mn_xO$ is not as qualitatively different from those in other II-VI diluted magnetic semiconductors as has been suggested. The singular electronic structure feature of $Zn_{1-x}Mn_xO$ is the presence of this $Mn^{2+/3+}$ ionization level within the gap, and the influence of this level on other physical properties of $Zn_{1-x}Mn_xO$ is discussed.

DOI: 10.1103/PhysRevB.82.115202 PACS number(s): 75.50.Pp, 73.50.Pz

I. INTRODUCTION

Diluted magnetic semiconductors (DMSs), such as II–VI semiconductors containing substitutional magnetic impurity ions, are widely researched for spin-based electronics (spintronics) or spin-photonics applications.[1,2] The defining feature of DMSs that makes them interesting for such applications is the existence of magnetic exchange coupling between delocalized, bandlike charge carriers and localized impurity spins, i.e., the so-called *sp-d* exchange interactions.[3–5] These interactions give rise to numerous technologically important properties, including giant magneto-resistance and Faraday rotation effects. The *sp-d* exchange energies are frequently determined optically by measurement of excitonic Zeeman splittings. A signature feature of DMSs is the dependence of the excitonic Zeeman splitting on the concentration and average magnetization of the embedded magnetic impurity ions. Within the mean-field and virtual crystal approximations, the balance between intrinsic and *sp-d* exchange contributions to the excitonic Zeeman splitting of a DMS can be described by Eq. (1).[5]

$$\Delta E_{Zeeman} = g_{int}\mu_B H + x_{eff}N_0(\alpha - \beta)\langle S_z\rangle. \quad (1)$$

The first term represents the intrinsic excitonic Zeeman splitting of the diamagnetic host semiconductor lattice, where g_{int} is the excitonic Landé splitting factor, μ_B is the Bohr magneton, and H is the strength of the applied magnetic field. The second term describes the contribution to the excitonic Zeeman splitting from the *sp-d* exchange interactions. This contribution depends on the effective dopant cation mole fraction (x_{eff}), the dopant spin expectation value in the direction of the applied magnetic field ($\langle S_z\rangle$, a negative value), and the mean dopant-carrier exchange energies ($N_0\alpha$ and $N_0\beta$ for conduction and valence band carriers, respectively). In Mn^{2+}-based II-VI DMSs, the *sp-d* term in Eq. (1) opposes the intrinsic excitonic Zeeman splitting, and is frequently one to two orders of magnitude greater than the intrinsic splitting at even modest values of x_{eff}. Consequently, Mn^{2+}-based II-VI DMSs typically show inverted and greatly enhanced values of ΔE_{Zeeman} relative to their corresponding diamagnetic II-VI parent compounds.

The applicability of the above general picture for $Zn_{1-x}Mn_xO$ remains in question. Interest in ZnO for spintronics was fueled by early predictions that *p*-doped $Zn_{1-x}Mn_xO$ could exhibit high-temperature ferromagnetism,[6–8] based on expectations that $Zn_{1-x}Mn_xO$ would have a larger *p-d* exchange energy ($N_0\beta$) than other II-VI DMSs because of its smaller lattice constant, a_0 ($N_0\beta \sim a_0^{-3}$).[4,8] Initial experimental estimates of *p-d* exchange energies obtained from analysis of x-ray absorption (XAS) and photoemission spectroscopic data seemed to support this expectation, yielding $N_0\beta \sim -2.7$ to -3.0 eV.[9,10] These values are comparable to but larger than those of other Mn^{2+}-based II-VI DMSs (for example, $N_0\beta = -1.1$ eV in $Zn_{1-x}Mn_xTe$ [11]). Subsequent magneto-photoluminescence measurements were interpreted as revealing small and perhaps even oppositely signed values of $N_0\beta$ in $Zn_{1-x}Mn_xO$, however, with $N_0(\alpha\text{-}\beta) \sim +0.10$ to $+0.16$ eV.[12,13] Assuming a typical value of $N_0\alpha \sim +0.2$ eV,[14,15] these measurements would imply $N_0\beta \sim +0.10$ to $+0.04$ eV, which would be anomalous in both sign and magnitude. Such observations have challenged our understanding of this material's electronic structure.

In parallel with these studies, other recent spectroscopic work has focused on elucidating the roles that TM photoionization levels play in determining the physical properties of $Zn_{1-x}TM_xO$ DMSs (TM=3*d* transition metal ion).[16–20] The frequent occurrence of such photoionization levels within the ZnO energy gap constitutes a key difference between

$Zn_{1-x}TM_xO$ and other II-VI DMSs, and it has been hypothesized that these ionization levels make major contributions to TM-carrier interactions in the ground states of the corresponding *n*- and *p*-type $Zn_{1-x}TM_xO$ materials.[16,17,21]

Despite many years of investigation, TM^{2+} photoionization in ZnO is still not fully understood. In general, two types of photoionization must be considered, the donor type [Eq. (2a)] and the acceptor type [Eq. (2b)]. These photoinduced transitions formally involve the transfer of charge carriers either to or from the TM^{2+} dopant, and are therefore sometimes referred to as charge-transfer (CT) transitions ($ML_{CB}CT$ and $L_{VB}MCT$, respectively).[16,18] Because of configuration interaction, the actual excited states observed experimentally involve mixing of the photoionization configurations [Eqs. (2a) and (2b)] with band-to-band configurations [Eq. (2c)]. The extent of band-to-band character mixed into the CT excited state depends on their energy difference, and it determines the CT transition's oscillator strength as well as the effective radius of the photogenerated bound carrier[16,22] (in an excited-state analog of the well-known inverse relationship between carrier binding energy and effective Bohr radius[23]).

$$ML_{CB}CT: \quad TM^{n+} \xrightarrow{h\nu} TM^{(n+1)+} + e^-_{CB} \tag{2a}$$

$$L_{VB}MCT: \quad TM^{n+} \xrightarrow{h\nu} TM^{(n-1)+} + h^+_{VB} \tag{2b}$$

$$\text{band-to-band:} \quad TM^{n+} \xrightarrow{h\nu} TM^{n+} + e^-_{CB} + h^+_{VB}. \tag{2c}$$

Considerable effort has been made recently to address the mid-gap electronic excited states of $Zn_{1-x}Mn_xO$ theoretically.[19,20,24,25] One interpretation invokes analogies to the Zhang-Rice singlet states of cuprates,[24] in which photogenerated valence-band holes are strongly exchange coupled to a Mn^{2+} ion. This model proposes explanations for the reversed sign and dramatically reduced magnitude of the apparent $N_0\beta$ measured spectroscopically, as well as the dependence of the energy gap on the magnetic ion concentration *x*. In contrast, time-dependent density-functional theory (TDDFT) calculations of the lowest-energy excited state in $Zn_{1-x}Mn_xO$ nanocrystals have suggested that the photogenerated hole is localized around the manganese ion in this state,[19] consistent with experimental descriptions.[16,17] Density-functional theorem (DFT) calculations employing a self-consistent band-structure correction also predict the presence of a mid-gap $Mn^{2+/3+}$ photoionization level.[25] Most recently, TDDFT results have suggested the possibility of spin-dependent hole delocalization among multiple Mn^{2+} ions in this excited state, the quantitative results of which were shown to favor parallel alignment of Mn^{2+} spins as described by a double-exchange Hamiltonian, i.e., an excited-state double-exchange magnetic polaron.[20]

In this paper, we describe characterization of paramagnetic $Zn_{1-x}Mn_xO$ thin films by various complementary spectroscopic techniques to elucidate the electronic structure of this material. As described previously,[16–18,26–33] doping with Mn^{2+} introduces a new broad absorption band within the ZnO optical gap. MCD spectroscopy demonstrates that this band is associated with isolated Mn^{2+} ions, not Mn_mO_n clusters or other special scenarios. Photoconductivity and valence band x-ray photoelectron spectroscopy (XPS) measurements are consistent with assignment of this new band as a donor-type $Mn^{2+/3+}$ photoionization transition. MCD spectroscopy also demonstrates that addition of Mn^{2+} inverts the sign of the ZnO excitonic Zeeman splitting and increases it by approximately one order of magnitude relative to ZnO, similar to what is typically seen in other Mn^{2+}-based II-VI DMSs. The contributions of the mid-gap $Mn^{2+/3+}$ photoionization level to other physical properties of $Zn_{1-x}Mn_xO$, including dopant-carrier exchange and carrier-mediated dopant-dopant magnetic exchange interactions, are also briefly discussed.

II. METHODS

Films were grown on double-sided or single epi-polished $10\times5\times0.5$ mm^3 *c*-plane $Al_2O_3(0001)$ using pulsed laser deposition from polycrystalline $Zn_{1-x}Mn_xO$ targets. Details of the film deposition procedure and conditions, as well as basic characterization, can be found in Refs. 34 and 35. Addition of Mn^{2+} increased the ZnO resistivity from $\sim$40–50 Ohm cm to $>10^9$ Ohm cm for $Zn_{1-x}Mn_xO$ ($x=0.002$ and 0.05).

Electronic absorption spectra were measured using a Cary 500 (Varian) spectrophotometer. The electronic absorption spectra shown here have been corrected for interference fringes by the method described in Ref. 36. MCD spectra were collected on films $\sim$100 nm thick using an Aviv 40DS spectropolarimeter and a high-field superconducting magneto-optical cryostat (Cryo-Industries SMC-1659 OVT) with a variable temperature sample compartment positioned in the Faraday geometry. For measurements on *c*-ZnO, the *c*-axis of the ZnO was oriented parallel to the magnetic field. MCD intensities were measured as differential absorbance, $\Delta A = A_L - A_R$, where A_L and A_R refer to the absorption of left (σ^-) and right (σ^+) circularly polarized light, following the sign convention of Piepho and Schatz.[37] MCD spectra were measured as θ(mdeg), where $\theta(\text{mdeg}) = 32{,}982\ \Delta A$. Most MCD spectra are reported as $\Delta A/A_0$, where ΔA is the MCD intensity, and A_0 is the absorbance at the band maximum. Particle induced x-ray emission (PIXE), Rutherford backscattering (RBS), XPS, and transmission electron microscopy (TEM) measurements were performed at Pacific Northwest National Laboratory. Dopant concentrations in thinner films were determined using PIXE. Film thicknesses were determined using RBS. XPS valence band spectra were acquired at normal take-off angle with a monochromatic Al K_α x-ray source ($h\nu=1486.6$ eV).

Photoconductivity spectra were measured by applying a bias to the film (0.100–200 V) using a Keithley 2400 sourcemeter. The light source was a tungsten halogen lamp dispersed through a 0.3 m monochromator equipped with a 600 gr/mm grating blazed at 500 nm and chopped at 10–50 Hz before the sample. The contacts were copper wires wrapped with indium pressed onto the film surface. Photocurrent action spectra were measured using lock-in amplification (Stanford Research 830). Very similar results were

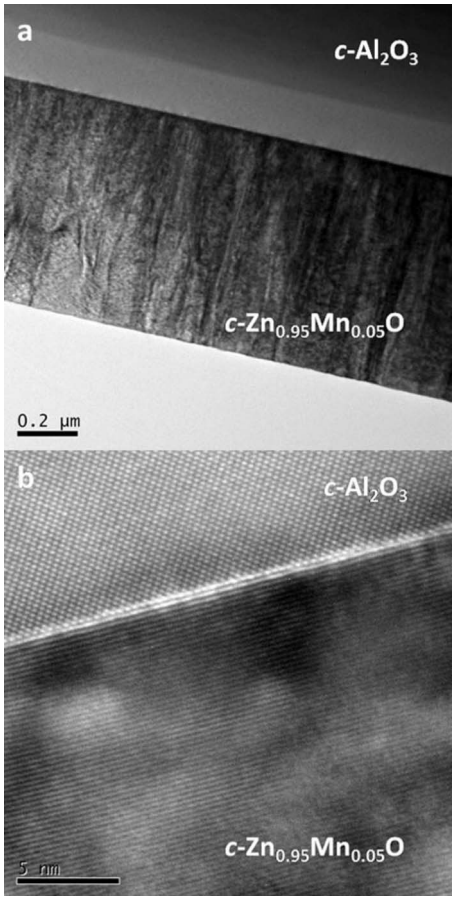

FIG. 1. TEM of c-$Zn_{0.95}Mn_{0.05}O$ on c-Al_2O_3 (a) Low magnification micrograph showing a smooth film deposited on c-Al_2O_3. (b) High-resolution micrograph of c-$Zn_{0.95}Mn_{0.05}O$ film and c-Al_2O_3 substrate interface.

obtained using continuous excitation without chopping, but with reduced signal-to-noise ratios. Room- and low-temperature photocurrent action spectra were measured inside a Janis flow optical cryostat. For low temperature measurements on $Zn_{1-x}Mn_xO$ films, samples were additionally illuminated with a constant white light source to increase conductivity.[38] All photoconductivity spectra have been corrected for the monochromator response and the excitation lamp intensity distribution.

III. RESULTS AND ANALYSIS

A. General characterization

Figure 1 shows TEM micrographs of a representative c-$Zn_{0.95}Mn_{0.05}O$ film grown on c-Al_2O_3. The TEM micrographs show a smooth, well-oriented, epitaxial film with columnar grains and a sharp interface at the substrate. All films described in this study thus have their c-axes oriented perpendicular to the substrate. By lacking substantial grain boundary defect densities, these $Zn_{1-x}Mn_xO$ samples differ from previous nanocrystalline samples in which absorption, MCD, and photocurrent action spectroscopies have been performed.[16,17]

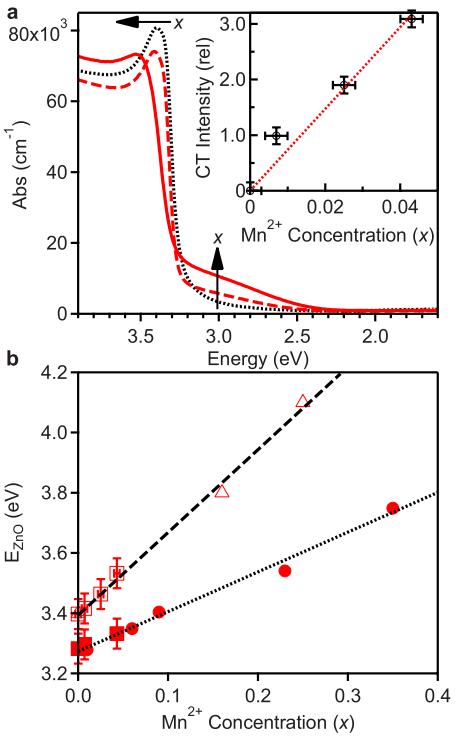

FIG. 2. (Color online) (a) Room-temperature electronic absorption spectra of c-ZnO and c-$Zn_{1-x}Mn_xO$ thin films, normalized for film thickness (··· ZnO, — $Zn_{0.957}Mn_{0.043}O$, −−− $Zn_{0.993}Mn_{0.007}O$). Inset: $ML_{CB}CT$ intensity vs Mn^{2+} concentration. (b) Energies of the first ZnO band-to-band absorption feature plotted vs x for the films shown in (a) (■ CT-intersect and □ band-maximum methods), and for various films from the literature [● (Ref. 29) CT-intersect; △ (Ref. 42) band-maximum]. ··· linear best fit, $E_{ZnO}=3.28+1.29x$ (eV). – – linear best fit, $E_{ZnO}=3.40+2.73x$ (eV).

B. Spectroscopic characterization

1. Electronic absorption spectroscopy

Figure 2(a) shows room-temperature electronic absorption spectra of three ZnO and $Zn_{1-x}Mn_xO$ ($x=0.007$ and 0.043) films, all ~100 nm thick. All three films show intense excitonic absorption maxima at ~3.4 eV. A blue shift of the excitonic absorption maximum is observed with increasing Mn^{2+} concentration. This shift has been observed previously for $Zn_{1-x}Mn_xO$ and other Mn^{2+}-based II-VI DMSs.[5,29,39] Below the exciton, a broad feature is observed tailing into the visible energy region in the $Zn_{1-x}Mn_xO$ films. In our previous studies, we have assigned this band as a $Mn^{2+/3+}$ donor-type photoionization ($ML_{CB}CT$) transition on the basis of optical electronegativity calculations,[16,17] but in other reports it has been attributed to d-d transitions,[9,26,27,30] an impurity phase,[31] an unspecified charge-transfer transition,[28,29] a $Mn^{2+/+}$ acceptor-type photoionization ($L_{VB}MCT$) transition,[40] or a mid-gap Zhang-Rice-like state.[24,33] By independent assessment, this band has also been assigned as a $Mn^{2+/3+}$ photoionization transition in Refs. 32 and 41. The data below strongly support this assignment, and the relationship between this description and the proposed Zhang-Rice-like description is discussed in Sec. IV.

Figure 2(b) plots the shift of the ZnO absorption energy with Mn^{2+} concentration. The open symbols show the ener-

gies of the first excitonic maxima of the films from Fig. 2(a), along with comparable literature data.[29,42] In some publications, this relationship has been analyzed by plotting the data as $(\alpha h\nu)^2$ vs $h\nu$ and determining where the ZnO and mid-gap features intersect.[29] Generally, this approach is necessitated when samples are too optically dense at the excitonic maximum. The solid symbols in Fig. 2(b) show the shift of the ZnO absorption onset with x determined in this way. Both methods give similar blue shifts versus x, but the shift of the maximum is considered more accurate because it is less sensitive to the changes in bandshape with x evident from Fig. 2(a), which influence the $(\alpha h\nu)^2$ analysis more substantially. We note that for undoped ZnO, the first exciton energy (E_{ZnO}) is smaller than E_g by the exciton binding energy of $\sim$60 meV.[43]

The blue shift of the ZnO band-to-band absorption upon addition of Mn^{2+} has been proposed to provide evidence of strong exchange coupling between valence band holes and localized spins of the Mn^{2+} ions, i.e., the Zhang-Rice-like state.[33] We do not subscribe to this interpretation of the data, and propose instead that this trend can be understood more simply by considering the energies of the cation valence orbitals that make up the conduction band. In ZnO, the conduction-band-edge wave function is predominantly Zn^{2+} 4*s* in character. The Mn^{2+} 4*s* orbitals are well above the ZnO CB edge and hence poorly aligned for resonance. The band gap widens as the Zn^{2+} 4*s* orbitals are replaced with nonresonant Mn^{2+} 4*s* orbitals. In support of this interpretation, we note that a very similar trend [$E_{ZnO}=3.26+1.57x$ (eV)] is also observed upon replacement of Zn^{2+} with Mg^{2+},[44] which has a large 4*s* energy mismatch but no unpaired spins and hence no possibility for formation of a Zhang-Rice-like state. The broadening of the band edge absorption with increasing x in Fig. 2(b) is attributable to inhomogeneous broadening due to spatial fluctuations in x.

The inset of Fig. 2(a) shows that when the Mn^{2+} concentration is increased, the mid-gap absorption intensity also increases proportionally. The room-temperature per-Mn^{2+} molar extinction coefficient determined from the $Zn_{0.957}Mn_{0.043}O$ film at 3.00 eV is $\varepsilon_{Mn,\perp} \approx 2000 \pm 700$ M^{-1} cm^{-1}, where the sizable uncertainty comes from the presence of interference fringes in addition to experimental uncertainties in Mn^{2+} concentration and film thickness. This value agrees reasonably well with that reported previously for colloidal $Zn_{0.989}Mn_{0.011}O$ nanocrystals ($\varepsilon_{Mn} \approx 950$ M^{-1} cm^{-1}) (Ref. 17) and for bulk $Zn_{1-x}Mn_xO$ single crystals ($\varepsilon_{Mn,\perp} \approx 1400$ M^{-1} cm^{-1} and $\varepsilon_{Mn,\parallel} \approx 1700$ M^{-1} cm^{-1}),[40] which may provide more reliable estimates because of the absence of interference fringes. For all samples, these ε_{Mn} values are much too large for this band to be attributed to Mn^{2+} *d-d* transitions. Mn^{2+} *d-d* transitions are spin forbidden and consequently very weak, with $\varepsilon_{Mn} \sim 1-10$ M^{-1} cm^{-1} at their maxima in $Zn_{1-x}Mn_xS$ (Ref. 45) and related tetrahedral Mn^{2+} coordination complexes.[46,47] Instead, the large extinction coefficient of this mid-gap absorption points to its assignment as a photoionization transition.

2. *Photoconductivity and x-ray photoelectron spectroscopies*

To characterize the mid-gap states in more detail, photoconductivity and XPS measurements were performed on the same $Zn_{1-x}Mn_xO$ films as described above. Figure 3 shows the room-temperature electronic absorption and variable-temperature photoconductivity action spectra of a $Zn_{0.975}Mn_{0.025}O$ film. As in the absorption spectrum, these photoconductivity action spectra are dominated by band-to-band transitions beginning at $\sim$3.1 eV and continuing to higher energies. The rollover in photocurrent response ($\sim$3.2 eV in the room temperature spectrum) has also been observed in many other semiconductors[48,49] and is due to recombination of carriers generated near the film surface in this high optical density regime. Following Varshni-like behavior, the band-edge photoconductivity shifts to higher energies as the temperature is lowered, and this shifts the surface recombination rollover in the photoconductivity spectra to higher energies as well.

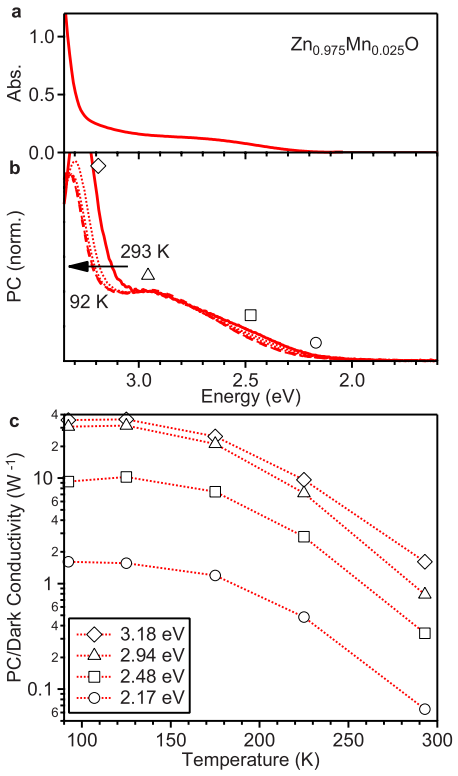

FIG. 3. (Color online) (a) Room-temperature electronic absorption spectrum and (b) variable-temperature photoconductivity action spectra (293, 225, 175, 125, and 92 K) of a *c*-$Zn_{0.975}Mn_{0.025}O$ thin film. The photoconductivity data have been normalized at 2.987 eV. (c) The ratio of photoconductivity (PC) to dark conductivity plotted vs temperature, measured at the various energies designated by the symbols in (b). The dotted lines are guides to the eye.

At lower energies, the action spectra clearly show photoconductivity coming from excitation into the mid-gap transition down to $\sim$2.2 eV. The observation of substantial photoconductivity with excitation into the broad mid-gap absorption band provides strong support for assignment of this feature as a photoionization transition that generates delocalized charge carriers. *d-d* excitations are generally highly localized, and therefore do not show photoconductivity without the involvement of charge-transfer states in the same energy region.[38,50] Although this mid-gap transition is clearly observed in photoconductivity measurements, its absorbed

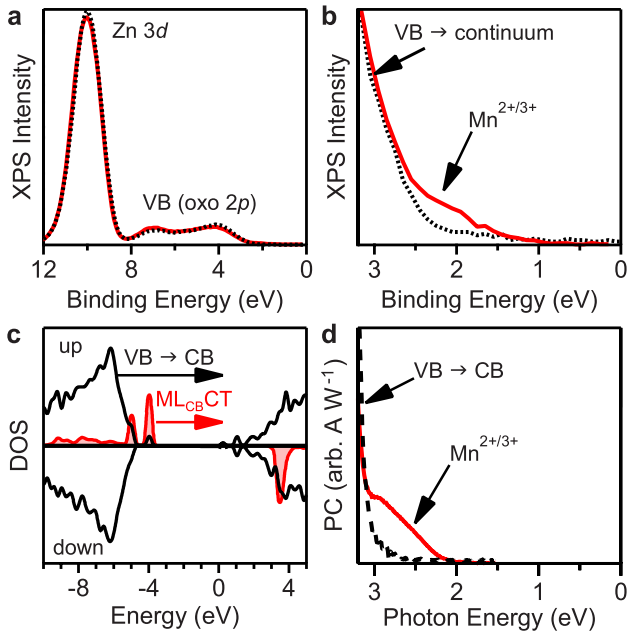

FIG. 4. (Color online) (a) Room-temperature valence band XPS spectra of $Zn_{0.98}Al_{0.02}O$ (···) and $Zn_{0.95}Mn_{0.05}O$ (—) films. (b) Data from (a) plotted on an expanded scale. (c) Calculated density of states (DOS) for a $Zn_{83}MnO_{84}$ cluster (~1.5 nm dia.), adapted from Ref. 19. The DOS are defined as the number of one-electron orbitals within a bin size of 0.2 eV. The shaded regions indicate the Mn^{2+} partial contributions (×10). Spin-up and spin-down densities are plotted as positive and negative values, respectively. The calculated energies do not match experiment because of the small cluster size considered in Ref. 19, but compare well with $Zn_{1-x}Mn_xO$ nanocrystal energies and extrapolate well to bulk energies. (d) Room-temperature photoconductivity spectra of ZnO and $Zn_{0.975}Mn_{0.025}O$ films, plotted on the same energy scale as (b).

photon-to-current conversion efficiency is only ~10% as large as that for the nearby band-to-band excitation, consistent with photogeneration of a more strongly bound charge carrier in this case. From the photoconductivity spectrum, we estimate a binding energy of ~0.94 eV for the photogenerated hole in this excited state.

The mid-gap photoconductivity does not change appreciably with temperature between room and cryogenic temperatures; the photoconductivity grows moderately relative to the dark conductivity as the temperature is lowered [Fig. 3(c)], because of the decrease in dark conductivity with decreasing temperature.

As described by Eqs. (2a) and (2b), charge-transfer transitions in $Zn_{1-x}Mn_xO$ could formally involve either transfer of an electron from the Mn^{2+} into the conduction band, or transfer of a valence band electron to the Mn^{2+}. To examine the direction of charge transfer in this mid-gap photoexcitation, we performed valence band XPS measurements. Whereas the photoconductivity experiment is sensitive to both types of photoionization, valence-band XPS measures excitation of electrons to the continuum, and thus selectively probes only occupied levels.

Figure 4(a) plots the valence-band XPS spectra of a $Zn_{0.95}Mn_{0.05}O$ film, in comparison with that of a reference $Zn_{0.98}Al_{0.02}O$ film. Figure 4(b) plots the same valence-band XPS spectra shown in Fig. 4(a) on an expanded scale. For comparison, Fig. 4(d) plots the photoconductivity action spectra of comparable ZnO and $Zn_{0.975}Mn_{0.025}O$ films on a similar scale. In both experiments, addition of Mn^{2+} introduces intensity just above the valence-band edge that is not seen in the reference ZnO sample. This similarity provides very strong evidence supporting the assignment of the mid-gap optical band as a donor-type photoionization of Mn^{2+} [i.e., the $ML_{CB}CT$ transition, Eq. (2a)].[16–18,20] The XPS and photoconductivity spectra resemble one another because both experiments probe excitation of Mn^{2+} electrons and nearby valence band electrons. The small energy differences between the two experiments are attributed in part to uncertainties in alignment of the XPS data, which has been referenced to the Fermi level (fixed to 0 eV) under the assumption that this resides close to the conduction band edge in these *n*-type ZnO films. The above interpretation is bolstered by density functional calculations, which suggest the presence of occupied Mn^{2+} *d* orbitals above the VB edge [Fig. 2(c), adapted from Ref. 19]. Although substantial differences between these one-electron orbital energies and the true transition energies are expected to result from final-state multielectron interactions, this DOS provides an intuitive relationship between the Mn^{2+}-based optical and XPS transitions and the presence of occupied Mn^{2+} *d* levels within the ZnO energy gap. It is also interesting to note that the threshold of this $Mn^{2+/3+}$ ionization determined optically agrees well with that determined by conductivity measurements (~2.0 eV at room temperature).[51]

We note that previous resonant XPS measurements have placed this Mn^{2+} *d* band ~1.5 eV *below* the VBM of ZnO,[9] whereas here it is identified just *above* the VBM. Location of the *d* levels below the VBM is an essential assumption behind the proposal of mid-gap Zhang-Rice-like states in $Zn_{1-x}Mn_xO$.[24] The XPS data of Ref. 9 and those reported here agree very well when aligned at the Zn 3d peak at ~10 eV, so the discrepancy rests only in how the VBM is defined. In ref. 9, the onset of XPS intensity in $Zn_{1-x}Mn_xO$ itself was used to define the VBM. In Fig. 2, the VBM is defined by the reference ZnO film. The good alignment of the ZnO XPS spectrum with the deeper levels of the $Zn_{1-x}Mn_xO$ spectrum [Fig. 4(a)] validates the procedure used here. The conclusion from this comparison is that the Mn^{2+} *d* levels reside ~0.5 eV *above* the VBM of ZnO, not ~1.5 eV below it. A similar placement was concluded from resonant x-ray emission measurements of $Zn_{1-x}Mn_xO$ pellets.[52] With this alignment, Mn^{2+} in ZnO should be considered as having a normal bonding scheme, contrasting with the inverted bonding scheme typical of Mn^{2+} in chalcogenide II-VI semiconductors.[53] It is conceivable that this new XPS intensity above the VBM could be instead interpreted as split-off VB levels that are antibonding with respect to deeper Mn^{2+} *d* levels in an inverted bonding scheme, as suggested by the Zhang-Rice analogy. The relationship between these two interpretations as they pertain to the wave function of the photogenerated hole in $Zn_{1-x}Mn_xO$ is discussed in more detail below.

3. Magnetic circular dichroism spectroscopy

Low-temperature electronic absorption and MCD spectra of two $Zn_{1-x}Mn_xO$ films are presented in Fig. 5, in compari-

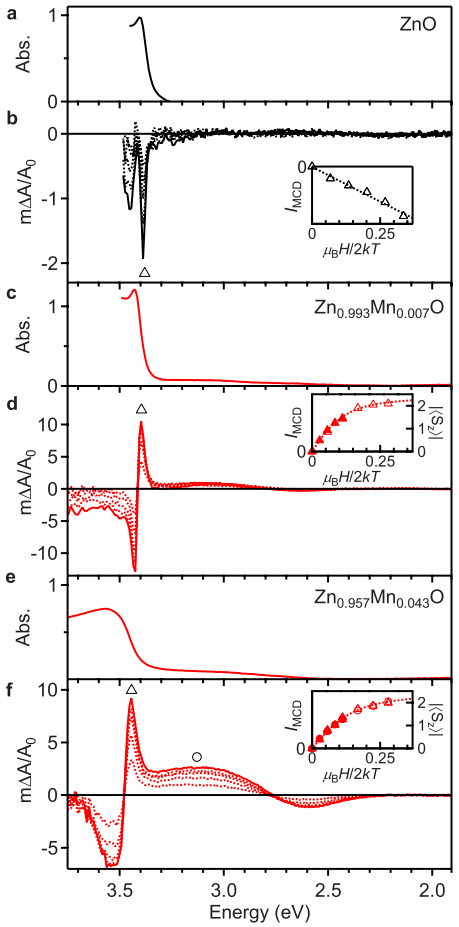

FIG. 5. (Color online) (a) 7 K electronic absorption spectrum and (b) 5 K, 1–5 T MCD spectra of a *c*-ZnO film. Inset: Magnetic field dependence of the leading-edge excitonic MCD intensity measured at 5 K (△), plotted vs $\mu_B H/2kT$. The dotted line is a linear fit to the data. (c) 6 K electronic absorption spectrum and (d) 6 K, 1–5 T MCD spectra of a $Zn_{0.993}Mn_{0.007}O$ film. Inset: Magnetic field dependence of the leading-edge excitonic MCD intensity measured at 6 K (△) and 12 K (▲), plotted vs $\mu_B H/2kT$. The dotted line shows the $S=5/2$ Brillouin function calculated at the same two temperatures. (e) 6 K electronic absorption spectrum and (f) 6 K, 1–5 T MCD spectra of a $Zn_{0.957}Mn_{0.043}O$ film. Inset: Magnetic field dependence of the leading-edge excitonic MCD intensity measured at 6 K (△) and 12 K (▲), and of the mid-gap $ML_{CB}CT$ intensity measured at 6 K (○) and 12 K (●) at the energies marked on the spectra, plotted vs $\mu_B H/2kT$. The dotted line is the calculated $S=5/2$ Brillouin function (scale on right ordinate).

son with reference spectra from a similar ZnO film. The absorption and MCD spectra of the ZnO film [Fig. 5(a) and 5(b)] show no features below ~3.3 eV. At ~3.4 eV, the characteristic ZnO excitonic maximum is observed in the absorption spectrum. Associated with this feature is a very weak MCD signal characterized by a negative leading-edge intensity, which indicates greater absorption of right (σ^+) circularly polarized light at lowest energy (see Methods for description of the sign convention used here). This ZnO MCD intensity increases linearly with applied magnetic field [inset, Fig. 5(b)].

TABLE I. MCD rotational strengths for ZnO and $Zn_{1-x}Mn_xO$ films. The value $(\Delta A'/A_0)\times(kT/\mu_B H)$ is proportional to the excitonic Zeeman splitting energy, ΔE_{Zeeman}. MCD values reported here are for the linear region before magnetic saturation (Curie region, $H=1$ T). Values for A_0 are taken from the absorption spectra shown in Figs. 5(a), 5(c), and 5(e), respectively.

	Transition type	Energy (eV)	$(\Delta A'/A_0)\times(kT/\mu_B H)$
ZnO	Exciton	3.388	−0.003
$Zn_{0.993}Mn_{0.007}O$	Exciton	3.397	+0.038
	$ML_{CB}CT$	3.054	+0.11
$Zn_{0.957}Mn_{0.043}O$	Exciton	3.444	+0.030
	$ML_{CB}CT$	3.054	+0.082

Introduction of Mn^{2+} leads to several important changes in the MCD spectrum. First, and most prominent, is the inversion of the leading-edge excitonic feature at ~3.4 eV, which becomes positive upon doping. Second, the excitonic MCD feature is much more intense in the $Zn_{1-x}Mn_xO$ films than in the ZnO film. Third, this excitonic MCD intensity no longer grows linearly with applied magnetic field as in ZnO [Fig. 5(b), inset], but now saturates at high magnetic fields and low temperatures [Figs. 5(d) and 5(f), insets] in a way characteristic of the $S=5/2$ ground state magnetization of Mn^{2+}. The blue shift of the excitonic transition upon Mn^{2+} doping is also clearly observed in the MCD spectra: whereas the leading-edge feature of the ZnO MCD spectrum is just below 3.39 eV [Fig. 5(b)], this feature shifts to 3.40 eV at $x=0.007$ [Fig. 5(d)] and to 3.44 eV at $x=0.043$ [Fig. 5(f)]. Similarly, the excitonic MCD feature broadens with increasing x, as observed by absorption (Fig. 2). Overall, these trends in bandshape and energy measured by MCD closely mimic those described above for absorption measurements.

Finally, the MCD spectra of the $Zn_{1-x}Mn_xO$ films all show a new broad negative pseudo-A term[37] feature tailing down to ~2.2 eV, i.e., in the energy range associated with the $ML_{CB}CT$ transition. On the high-energy side, this new band overlaps the sharp ZnO excitonic feature. Importantly, the intensity of this MCD feature also reflects $S=5/2$ saturation magnetization [Fig. 5(f), inset], indicating that it is a transition associated with magnetically isolated $S=5/2$ Mn^{2+} ions.

4. Spectroscopic evidence of sp-d exchange interactions in $Zn_{1-x}Mn_xO$

To compare the MCD data of ZnO and $Zn_{1-x}Mn_xO$ on a more quantitative basis, the ratios of MCD to absorption intensities of the major features in Fig. 5 in the low-field (Curie) limit are tabulated in Table I as $\Delta A'/A_0$, where $\Delta A'$ and A_0 are defined as the MCD and absorption intensities at the band maxima, respectively, as detailed in Refs. 37 and 54. The data in Table I have been corrected for the small difference in experimental conditions between samples ($kT/\mu_B H$ factor). For a given sample, $\Delta A'/A_0$ at the leading-edge excitonic feature is proportional to the excitonic Zeeman splitting energy, ΔE_{Zeeman}. Direct comparison of $\Delta A'/A_0$ be-

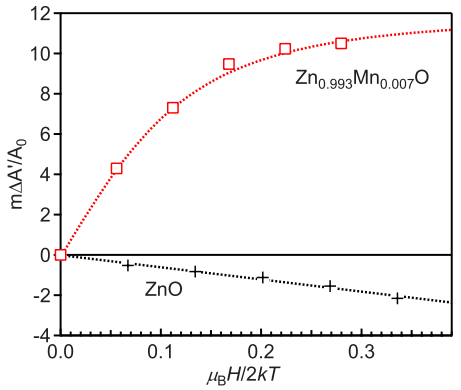

FIG. 6. (Color online) Magnetic field dependence of the leading edge excitonic MCD intensity feature of *c*-ZnO (+) and *c*-$Zn_{0.993}Mn_{0.007}O$ (□) thin films, measured at 5 and 6 K, respectively, and plotted as $\Delta A'/A_0$ vs $\mu_B H/2kT$. The dotted lines show the $S=5/2$ Brillouin function ($Zn_{0.993}Mn_{0.007}O$ film) and a linear function (ZnO film).

tween two related samples is therefore a useful model-independent measure of their relative ΔE_{Zeeman} magnitudes, provided the two samples have similar absorption band shapes. The excitonic feature of the $x=0.043$ film is substantially broader than those of the other two films, so we focus on comparison of the ZnO and $Zn_{0.993}Mn_{0.007}O$ results. The ratios $\Delta A'/A_0$ for ZnO and $Zn_{0.993}Mn_{0.007}O$ films are plotted vs $\mu_B H/2kT$ in Fig. 6. From Table I and Fig. 6, $\Delta A'/A_0$ for the first excitonic feature of the $Zn_{0.993}Mn_{0.007}O$ film is one order of magnitude greater than in the ZnO reference sample, and opposite in sign. From the optical selection rules for circularly polarized absorption, the negative sign of the first excitonic MCD feature in ZnO indicates $g_{int}>0$. The positive leading edge MCD intensity for $Zn_{1-x}Mn_xO$ reflects a reversal in the sign of the excitonic Zeeman splitting at the band edge, and hence an inversion of g_{eff} upon doping. The inversion of the excitonic MCD intensity and its enhancement by an order of magnitude are typical of TM^{2+}-based II-VI DMSs, and are characteristic signatures of excitonic Zeeman splittings dominated by *sp-d* exchange with $N_0(\alpha-\beta)>0$.[5,55]

The above discussion describes model-independent analysis of relative values of ΔE_{Zeeman}. As emphasized by others previously,[24,56,57] absolute quantification of ΔE_{Zeeman} (or $N_0\beta$) in $Zn_{1-x}TM_xO$ DMSs from magneto-optical data is complicated by uncertainties in the valence band structure of ZnO and the likelihood of overlapping excitonic features. Additionally, Fig. 2 shows that these excitonic features broaden with doping, which also complicates quantitative analysis. Finally, Fig. 2 shows spectral overlap of the excitonic and photoionization bands, which complicates quantitative analysis of the excitonic MCD intensities. We therefore refrain from estimating $N_0\beta$ itself from these data, and simply conclude that the data in Figs. 5 and 6 indicate that the major qualitative aspects of excitonic *sp-d* exchange found in other Mn^{2+}-based II-VI DMSs are retained in $Zn_{1-x}Mn_xO$. In particular, the data do not allow confirmation of the proposal that the *p-d* exchange integral has changed sign from negative (antiferromagnetic) to positive

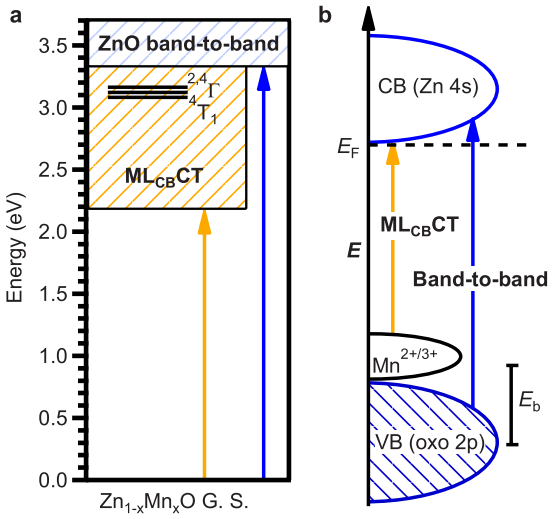

FIG. 7. (Color online) (a) Energy level scheme for $Zn_{1-x}Mn_xO$, showing the CT and band-to-band transitions. The empirically predicted energies of the Mn^{2+} *d-d* transitions are included for reference. (b) Schematic one-electron density of states for $Zn_{1-x}Mn_xO$, depicting the approximate transitions from (a) in a one-electron scheme. The split-off Mn^{2+}-derived band yields partial hole localization at Mn^{2+} with a binding energy of E_b following $ML_{CB}CT$ excitation, analogous to a Zhang-Rice band.

(ferromagnetic).[24] We note that strong *sp-d* exchange was already concluded for $Zn_{1-x}Co_xO$ in earlier optical MCD studies of that material,[56,58] but this conclusion was questioned in light of subsequent results.[24,59,60]

Overall, the MCD results presented here suggest that even apparent excitonic *sp-d* exchange splittings in $Zn_{1-x}Mn_xO$ are not as qualitatively different from those of other Mn^{2+}-based DMSs as has been thought. Beyond this conclusion, we suggest that concern over the magnitudes of the excitonic Zeeman splitting and *p-d* exchange energies may even be somewhat misplaced, at least with respect to potential magnetic/spin-electronics properties and magneto-photoluminescence of $Zn_{1-x}Mn_xO$, because unlike other Mn^{2+}-based II-VI DMSs, many of the physical properties of $Zn_{1-x}Mn_xO$ are not predominantly determined by such *sp-d* exchange interactions but instead are dominated by the presence of the mid-gap $Mn^{2+/3+}$ ionization band, as discussed below.

IV. DISCUSSION

Figure 7 summarizes the electronic structure of $Zn_{1-x}Mn_xO$ deduced from the data presented above. Figure 7(a) shows the excited state energies relative to the electronic ground state. The lowest electronic excited state in $Zn_{1-x}Mn_xO$ possesses donor-type photoionization ($ML_{CB}CT$) character and gives rise to photoconductivity. Above the $ML_{CB}CT$ origin are several Mn^{2+} *d-d* transitions that carry very little oscillator strength and have, to date, not been detected in $Zn_{1-x}Mn_xO$ by either absorption or photoluminescence (PL) techniques. These *d-d* bands are masked by the much more intense CT band. At even higher energies are the interband transitions of the ZnO host. These transitions over-

lap the CT band in the energy spectrum, and therefore cannot be neglected when analyzing the ZnO energy gap optically or when analyzing magnetoreflectance or MCD spectra.

A. Mn^{2+} *d-d* transitions and intracenter photoluminescence

Whereas wide-gap Mn^{2+}-based II-VI DMSs such as $Zn_{1-x}Mn_xS$ and $Zn_{1-x}Mn_xSe$ typically show the characteristic $^4T_1(G) \rightarrow {}^6A_1$ luminescence band of Mn^{2+} at energies $\sim$2.1 eV, no such PL has been reported for $Zn_{1-x}Mn_xO$, despite its 3.4 eV energy gap. Mn^{2+}-based PL was also not observed in the present investigations. We have previously proposed that the intra-Mn^{2+} PL is not observed in $Zn_{1-x}Mn_xO$ because the $^4T_1(G)$ electronic origin resides above the onset of the $ML_{CB}CT$ band, introducing new and rapid nonradiative deactivation channels.[17,61] The $^4T_1(G)$ and higher *d-d* excited states of $Zn_{1-x}Mn_xO$ have never been observed spectroscopically, but their energies can be estimated empirically.[17] To do so, we have considered homologous TM=Mn^{2+}, Co^{2+}, and Ni^{2+} compounds of the halides, $[TMX_4]^{2-}$ (X=Cl,Br,I), for which the Mn^{2+} *d-d* energies are well characterized using ligand field theory.[46,62,63] From experimental ligand-field parameters Dq and B for these compounds, and the experimental values of Dq and B for $Zn_{1-x}Co_xO$ and $Zn_{1-x}Ni_xO$,[64] values of $10Dq \approx 0.52$ eV and $B \approx 74$ meV for $Zn_{1-x}Mn_xO$ are estimated. A value of $C/B = 6.5$ was estimated for $Zn_{1-x}Mn_xO$ from the same literature data. The $Zn_{1-x}Mn_xO$ ligand-field parameters estimated independently from the Co^{2+} and Ni^{2+} homologs agree well with one another.

Using these empirical parameters and the d^5 Tanabe-Sugano matrices, the energies of the first several Mn^{2+} *d-d* electronic excited states of $Zn_{1-x}Mn_xO$ above the $^6A_1$ ground state were calculated. The *d-d* excited-state energies of $Zn_{1-x}Mn_xO$ estimated by this method are: $^4T_1(G)$ 3.08 eV, $^4T_2(G)$ 3.13 eV, ^4E, and $^4A_1(G)$ 3.14 eV.[17] These *d-d* excited states are included in Fig. 7 for comparison with the other excited states discussed above. To gauge the accuracy of this empirical approach, we have applied the same method to calculate the *d-d* excited-state energies in $Zn_{1-x}Mn_xS$, for which experimental data exist.[45] The calculated (vs experimental) energies for this lattice are: 2.07 (2.31), 2.27 (2.49), and 2.38 (2.67) eV. The empirically estimated energies all agree with the experimental numbers to within $\sim$10%, lending credence to the conclusion that the first *d-d* excited state of Mn^{2+} should occur at substantially higher energy in ZnO than in other II-VI lattices. For comparison, cluster model calculations have estimated these $Zn_{1-x}Mn_xO$ *d-d* excited states to occur at 2.55, 2.85, 2.97, and 2.99 eV, respectively,[9] or $\sim$0.5 eV lower in energy than the empirical estimates but still well above the $ML_{CB}CT$ threshold of $\sim$2.2 eV.

The major contribution to the $^6A_1 \rightarrow {}^4T_1(G)$ transition energy comes from terms in the Hamiltonian beyond the single-particle approximation, i.e., the Coulomb and exchange energies. The Mn^{2+} *d-d* excited states occur at higher energies in ZnO than in other II-VI lattices because of the smaller covalency of the Mn^{2+}-O^{2-} bond than Mn^{2+}-S^{2-}, Se^{2-}, or Te^{2-} bonds, which limits the nephelauxetic reduction of electron-electron repulsion at the manganese ion. The conclusion of less covalent bonding in ZnO than in other II-VI DMSs is anticipated from simple electronegativity considerations, and is experimentally well established from comparison of Mn^{2+} hyperfine coupling constants obtained from EPR spectroscopy across this series: $|A| \sim 75 \times 10^{-4}$ cm^{-1} in $Zn_{1-x}Mn_xO$, compared to $\sim$65, 62, and 56×10^{-4} cm^{-1} in $Zn_{1-x}Mn_xS$, $Zn_{1-x}Mn_xSe$, and $Zn_{1-x}Mn_xTe$, respectively.[54,65–67]

Overall, these high *d-d* transition energies place the first *d-d* excited state of $Zn_{1-x}Mn_xO$ well within the CT manifold. Because transition metal compounds usually only emit from their lowest excited state, if at all, this energy ordering explains the absence of Mn^{2+} *d-d* photoluminescence in $Zn_{1-x}Mn_xO$ despite its presence in all other Mn^{2+}-based II-VI DMSs with sufficiently wide energy gaps. An interesting question arises whether PL from the CT band might be observed, but such transitions often relax nonradiatively with high efficiency because of strong electron-nuclear coupling.

As a corollary, it is worth noting that any excitonic PL observed from dilute $Zn_{1-x}Mn_xO$ must be dominated by regions of low Mn^{2+} local concentration, where energy relaxation is slowest and consequently the excitonic state has the highest probability of radiative recombination. Magneto-PL measurements can therefore provide only lower-limit estimates of *sp-d* exchange energies in this DMS. Values of $N_0\beta$ derived from magneto-PL[13] may be influenced by such a scenario.

B. Relationship of the $Zn_{1-x}Mn_xO$ charge-transfer state to Zhang-Rice singlets and excited-state double exchange

Several recent theoretical works have described the mid-gap optical band of $Zn_{1-x}Mn_xO$.[19,20,24,60] One of these[24] has proposed that it corresponds to a Zhang-Rice singlet analog rather than to the photoionization assignment described in ref. 16 and above. We suggest that the two descriptions are more similar than different. Specifically, it was proposed in ref. 16 that the existence of this optical band within the ZnO gap implies partial excited-state hole localization at Mn^{2+}, with an estimated Mn^{2+}-hole binding energy of $E_b \sim 0.42$ eV and an effective Bohr radius of $r_B \sim 0.45$ nm. The hole was, thus, concluded to have substantial valence band character, and the excited state was concluded to be best described as a *mixture* of two electronic configurations: $d^4 + e^-_{CB}$ *and* $d^5 + e^-_{CB} + h^+_{VB}$ [Eq. (4) in Ref. 16]. In Ref. 24, this transition is described as $d^5 \rightarrow d^5 + e^-_{CB} + h^+_{VB}$, with strong coupling between the photogenerated holes and localized *d* spins leading to hole localization, and a distinction is made between this and the $d^5 \rightarrow d^4 + e^-_{CB}$ configuration. The analogy was drawn to the Zhang-Rice singlets of cuprates, in which a photogenerated oxide hole is strongly exchange coupled to a Cu^{2+} spin. In both the Zhang-Rice-like and $ML_{CB}CT$ descriptions of the mid-gap states in $Zn_{1-x}Mn_xO$, this transition involves promotion of an electron from the MnO_4 unit of $Zn_{1-x}Mn_xO$ into the conduction band. In both descriptions, this promotion is of a majority-spin electron (in the $ML_{CB}CT$ description, only a majority-spin Mn^{2+} electron can be excited into the conduction band because Mn^{2+} pos-

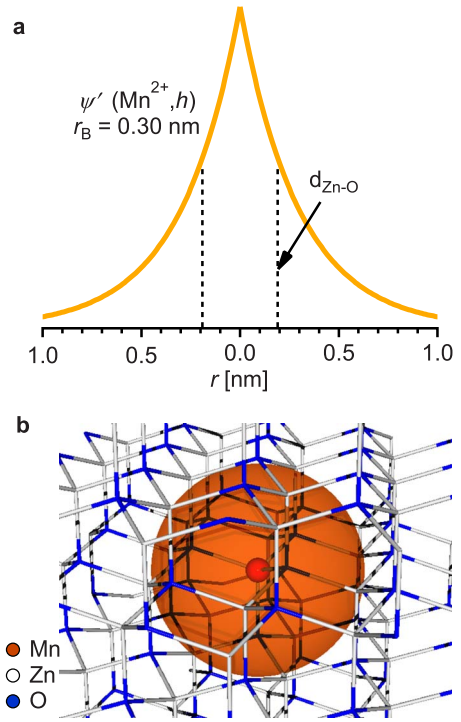

FIG. 8. (Color online) Hole wave function in the first electronic excited state of $Zn_{1-x}Mn_xO$, calculated assuming a hydrogenic 1*s* orbital with an effective Bohr radius of r_B=0.30 nm. (a) Wave function amplitude plotted vs distance from Mn^{2+}. (b) Wave function contour at radius r_B=0.30 nm from Mn^{2+}, superimposed onto the $Zn_{1-x}Mn_xO$ lattice. For comparison, the average ZnO bond length is 0.19 nm and the Zn-Zn nearest neighbor distance is 0.32 nm.

sesses no minority-spin electrons), in both descriptions, the photogenerated hole density has a manganese ion at its center, and in both descriptions, the hole wave function is greatly contracted around the manganese ion relative to a free valence-band hole. In our opinion, therefore, the clear distinction made in Ref. 24 between "$d^5+e^-+h^+$" and "d^4+e^-" excited-state configurations is not entirely satisfying because this excited state is best described as a mixture of these limiting configurations.[16] In some ways, the distinction between Zhang-Rice-like and $Mn^{2+/3+}$ photoionization assignments is one of perspective, because both arrive at similar excited-state wave function descriptions. The point where a concrete distinction can be made is in the conclusion of normal vs inverted bonding schemes. The experimental data here, as well as various recent DFT results,[19,20,25] point to a normal bonding scheme for $Zn_{1-x}Mn_xO$ in which the ZnO VBM resides below the majority-spin Mn^{2+} *d* orbitals. The mid-gap excited state of $Zn_{1-x}Mn_xO$ is thus most appropriately designated as deriving from a $Mn^{2+/3+}$ photoionization ($ML_{CB}CT$) transition.

From the onset of photoconductivity at ~2.2 eV measured in the epitaxial films studied here [Fig. 4(d)], we estimate a slightly larger h^+_{VB} binding energy ($E_b \sim 0.94$ eV) than was estimated in Ref. 16, which corresponds to $r_B \sim 0.30$ nm instead of $r_B \sim 0.45$ nm. Importantly, these effective radii are both on the same order of magnitude as the cation-cation nearest-neighbor distance of ~0.32 nm in ZnO. Figure 8 illustrates the hole wave function at the $ML_{CB}CT$ electronic origin schematically as a hydrogenic 1*s* orbital centered at the manganese with r_B=0.30 nm. Because of the extension of this wave function beyond the cation's first coordination sphere, one may anticipate relatively facile hole migration to nearby manganese ions or between manganese and other shallow acceptors in this excited state.

Linear-response TDDFT calculations support the description of the first electronic excited state in $Zn_{1-x}Mn_xO$ as a Mn^{2+}-based $ML_{CB}CT$ transition.[19,20] Calculations on $Zn_{1-x}Mn_xO$ clusters of various sizes predict a Mn^{2+}-centered excitation ~0.7 eV below the first band-to-band excitation in bulk $Zn_{1-x}Mn_xO$. This mid-gap excited state is predicted to involve conduction-band-like electrons and manganese-bound holes that have over 50% Mn 3*d* character and effective radii $< \sim 0.5$ nm. Interestingly, TDDFT calculations also predict excited-state spin-dependent hole delocalization in the presence of additional non-neighboring Mn^{2+} ions, with results that conform to the Anderson-Hasegawa double-exchange Hamiltonian.[20]

C. Relationship of the $Zn_{1-x}Mn_xO$ charge-transfer excited state to ground-state magnetism in *p*-doped $Zn_{1-x}Mn_xO$

As emphasized in Ref. 16, analysis of hole localization in the $ML_{CB}CT$ excited state of $Zn_{1-x}Mn_xO$ is also informative about scenarios that can be anticipated for the interaction of holes with Mn^{2+} ions in the *ground-state* of *p*-type $Zn_{1-x}Mn_xO$. The effective radius of the photogenerated hole in the $ML_{CB}CT$ electronic excited state of $Zn_{1-x}Mn_xO$ can be estimated from the energy of that state and is far smaller than that of a free hole in ZnO, but far greater than that of a Mn^{3+} *d* orbital, as described by resonance between the two configurations in Eq. (3a). Likewise, partial hole trapping in *p*-doped $Zn_{1-x}Mn_xO$ is described as intermediate between the localized and delocalized configurations of Eq. (3b).

$$Mn^{2+} + e^-_{CB} + h^+_{VB} \leftrightarrow Mn^{3+} + e^-_{CB} \tag{3a}$$

$$Mn^{2+} + h^+_{VB} \leftrightarrow Mn^{3+}. \tag{3b}$$

Zener-type *p-d* exchange represents the weak-interaction end of this continuum [left side of Eqs. (3a) and (3b)]. Because of the normal rather than inverted bonding scheme of Mn^{2+} in ZnO, the Mn^{2+}-hole interaction is much greater in $Zn_{1-x}Mn_xO$, i.e., toward the right in Eqs. (3a) and (3b). Strong Mn^{2+}-hole interactions of the type seen in $Zn_{1-x}Mn_xO$ can be expected to lead to interesting differences in magnetic and other physical properties. In *p*-doped $Zn_{1-x}Mn_xO$, the holes are sufficiently delocalized to interact with other Mn^{2+} ions in the lattice, and may lead to spin-dependent inter-Mn^{2+} hole delocalization akin to Zener's double exchange. Likewise, these holes can also interact with other shallow acceptors. The presence of a $Mn^{2+/3+}$ level close above the valence band edge of $Zn_{1-x}Mn_xO$ thus lends itself to spin-dependent hole delocalization, magnetic polaron formation, and potentially formation of a spin-split impurity band in *p*-type $Zn_{1-x}Mn_xO$ doped with shallow acceptors.

V. SUMMARY

In general terms, the defining characteristic of any DMS is the existence of giant spin splittings of the semiconductor band structure arising from Zener-type *sp-d* exchange interactions. The magnetic circular dichroism results presented here demonstrate that the excitonic Zeeman splittings of $Zn_{1-x}Mn_xO$ indeed show all of the hallmarks of *sp-d* exchange typical of other Mn^{2+}-based II-VI DMSs. This result suggests that the *sp-d* exchange interactions themselves in excitonic excited states of $Zn_{1-x}Mn_xO$ may not be as qualitatively different from those of other Mn^{2+}-based II-VI DMSs as has been thought.

Among Mn^{2+}-based II-VI DMSs, however, the singular electronic structure feature that makes $Zn_{1-x}Mn_xO$ unique is its display of a mid-gap $Mn^{2+/3+}$ ionization level. Understanding this unique electronic structure feature is essential to understanding the physical properties of this DMS. Using a combination of electronic absorption, magnetic circular dichroism, valence band X-ray photoelectron, and photoconductivity action spectroscopies, the assignment of this mid-gap transition as a $Mn^{2+/3+}$ photoionization ($ML_{CB}CT$) transition is strongly supported. Recent theoretical proposals of Zhang-Rice singlet analogs arising from strong excited-state hole-Mn^{2+} interactions have been largely reconciled with this experimental description of the mid-gap excited state, except on the point of normal vs inverted bonding schemes. These experimental results point to a normal bonding scheme in $Zn_{1-x}Mn_xO$, in contrast with other Mn^{2+}-based II-VI DMSs. Finally, the relationship between hole-Mn^{2+} interactions in $Zn_{1-x}Mn_xO$ involving photogenerated (in the $ML_{CB}CT$ excited state) and chemically generated (*p*-doping) holes has been briefly discussed. Whereas Zener-type *p-d* exchange can be observed in excitonic excited states, an important consequence of this electronic structure is that the Zener-type *p-d* hole-Mn^{2+} exchange is not operative in the lowest electronic excited state of $Zn_{1-x}Mn_xO$ or in the ground state of *p*-doped $Zn_{1-x}Mn_xO$, where it is instead replaced by a stronger and more localized hole-Mn^{2+} interaction.[16,24,60] $Zn_{1-x}Mn_xO$ is thus unique among Mn^{2+}-based II-VI DMSs because of its mid-gap $Mn^{2+/3+}$ level, which gives rise to a rich variety of unusual electronic and magnetic properties. Proposals to use $Zn_{1-x}Mn_xO$ for spin-based information processing must therefore address the roles of the Mn^{3+} configurations shown in Eq. (3) when considering magnetic ordering, carrier spin polarization, or spin transport in this material.

ACKNOWLEDGMENTS

This work was supported by the U.S. National Science Foundation (Grant No. CHE 0628252-CRC). Additional support to D.G. from the Sloan Foundation is gratefully acknowledged. A portion of the research was performed using EMSL, a national scientific user facility sponsored by the Department of Energy's Office of Biological and Environmental Research located at Pacific Northwest National Laboratory. Work performed at EMSL was supported by the U.S. Department of Energy, Office of Science, Office of Basic Energy Sciences, Division of Materials Science and Engineering Physics. We thank Chongmin Wang (EMSL) for the TEM measurements.

*gamelin@chem.washington.edu

[1] S. A. Wolf, D. D. Awschalom, R. A. Buhrman, J. M. Daughton, S. v. Molnar, M. L. Roukes, A. Y. Chtchelkanova, and D. M. Treger, Science **294**, 1488 (2001).
[2] S. J. Pearton, D. P. Norton, R. Frazier, S. Y. Han, C. R. Abernathy, and J. M. Zavada, IEE Proc.: Circuits Devices Syst. **152**, 312 (2005).
[3] P. Kacman, Semicond. Sci. Technol. **16**, R25 (2001).
[4] J. Blinowski, P. Kacman, and T. Dietl, in *Materials Research Society*, edited by T. J. Klemmer, J. Z. Sun, A. Fert, and J. Bass (Materials Research Society, Boston, Massachusetts, 2001), p. 109.
[5] *Diluted Magnetic Semiconductors*, edited by J. K. Furdyna and J. Kossut (Harcourt Brace Jovanovich, San Diego, 1988).
[6] K. Sato and H. Katayama-Yoshida, Physica E (Amsterdam) **10**, 251 (2001).
[7] T. Dietl, H. Ohno, F. Matsukura, J. Cibert, and D. Ferrand, Science **287**, 1019 (2000).
[8] T. Dietl, H. Ohno, and F. Matsukura, Phys. Rev. B **63**, 195205 (2001).
[9] T. Mizokawa, T. Nambu, A. Fujimori, T. Fukumura, and M. Kawasaki, Phys. Rev. B **65**, 085209 (2002).
[10] J. Okabayashi, K. Ono, M. Mizuguchi, M. Oshima, Subhra Sen Gupta, D. D. Sarma, T. Mizokawa, A. Fujimori, M. Yuri, C. T. Chen, T. Fukumura, M. Kawasaki, and H. Koinuma, J. Appl. Phys. **95**, 3573 (2004).
[11] A. Twardowski, P. Swiderski, M. von Ortenberg, and R. Pauthenet, Solid State Commun. **50**, 509 (1984).
[12] E. Przeździecka, E. Kamińska, E. Dynowska, W. Dobrowolski, R. Jakiela, Ł. Kłopotowski, M. Sawicki, M. Kiecana, and J. Kossut, Phys. Status Solidi C **3**, 988 (2006).
[13] E. Przeździecka, E. Kamińska, M. Kiecana, M. Sawicki, Ł. Kłopotowski, W. Pacuski, and J. Kossut, Solid State Commun. **139**, 541 (2006).
[14] T. Andrearczyk, J. Jaroszyñski, G. Grabecki, T. Dietl, T. Fukumura, and M. Kawasaki, Phys. Rev. B **72**, 121309 (2005).
[15] S. T. Ochsenbein, Y. Feng, K. M. Whitaker, E. Badaeva, W. K. Liu, X. Li, and D. R. Gamelin, Nat. Nanotechnol. **4**, 681 (2009).
[16] K. R. Kittilstved, W. K. Liu, and D. R. Gamelin, Nature Mater. **5**, 291 (2006).
[17] N. S. Norberg, K. R. Kittilstved, J. E. Amonette, R. K. Kukkadapu, D. A. Schwartz, and D. R. Gamelin, J. Am. Chem. Soc. **126**, 9387 (2004).
[18] K. R. Kittilstved and D. R. Gamelin, J. Appl. Phys. **99**, 08M112 (2006).
[19] E. Badaeva, C. M. Isborn, Y. Feng, S. T. Ochsenbein, D. R. Gamelin, and X. Li, J. Phys. Chem. C **113**, 8710 (2009).
[20] Y. Feng, E. Badaeva, D. R. Gamelin, and X. Li, J. Phys. Chem.

Lett. **1**, 1927 (2010).
[21] D. A. Schwartz, N. S. Norberg, Q. P. Nguyen, J. M. Parker, and D. R. Gamelin, J. Am. Chem. Soc. **125**, 13205 (2003).
[22] W. K. Liu, G. M. Salley, and D. R. Gamelin, J. Phys. Chem. B **109**, 14486 (2005).
[23] B. I. Shklovskii, Sov. Phys. Semicond. **6**, 1053 (1972).
[24] T. Dietl, Phys. Rev. B **77**, 085208 (2008).
[25] H. Raebiger, S. Lany, and A. Zunger, Phys. Rev. B **79**, 165202 (2009).
[26] C. H. Bates, W. B. White, and R. Roy, J. Inorg. Nucl. Chem. **28**, 397 (1966).
[27] D. Fichou, J. Pouliquen, J. Kossanyi, M. Jakani, G. Campet, and J. Claverie, J. Electroanal. Chem. **188**, 167 (1985).
[28] M. Jakani, G. Campet, J. Claverie, D. Fichou, J. Pouliquen, and J. Kossanyi, J. Solid State Chem. **56**, 269 (1985).
[29] T. Fukumura, Z. Jin, A. Ohtomo, H. Koinuma, and M. Kawasaki, Appl. Phys. Lett. **75**, 3366 (1999).
[30] Z.-W. Jin, Y.-Z. Yoo, T. Sekiguchi, T. Chikyow, H. Ofuchi, H. Fujioka, M. Oshima, and H. Koinuma, Appl. Phys. Lett. **83**, 39 (2003).
[31] J. R. Neal, A. J. Behan, R. M. Ibrahim, H. J. Blythe, M. Ziese, A. M. Fox, and G. A. Gehring, Phys. Rev. Lett. **96**, 197208 (2006).
[32] M. Godlewski, A. Wójcik-Głodowska, E. Guziewicz, S. Yatsunenko, A. Zakrzewski, Y. Dumont, E. Chikoidze, and M. R. Phillips, Opt. Mater. **31**, 1768 (2009).
[33] V. I. Sokolov, A. V. Druzhinin, N. B. Gruzdev, A. Dejneka, O. Churpita, Z. Hubicka, L. Jastrabik, and V. Trepakov, Phys. Rev. B **81**, 153104 (2010).
[34] T. C. Kaspar, T. Droubay, S. M. Heald, P. Nachimuthu, C. M. Wang, V. Shutthanandan, C. A. Johnson, D. R. Gamelin, and S. A. Chambers, New J. Phys. **10**, 055010 (2008).
[35] T. C. Droubay, D. J. Keavney, T. C. Kaspar, S. M. Heald, C. M. Wang, C. A. Johnson, K. M. Whitaker, D. R. Gamelin, and S. A. Chambers, Phys. Rev. B **79**, 155203 (2009).
[36] F. R. S. Clark and D. J. Moffatt, Appl. Spectrosc. **32**, 547 (1978).
[37] S. B. Piepho and P. N. Schatz, *Group Theory in Spectroscopy with Applications to Magnetic Circular Dichroism* (Wiley, New York, 1983).
[38] N. V. Joshi, *Photoconductivity: Art, Science, and Technology* (Dekker, New York, 1990).
[39] R. Viswanatha, S. Sapra, S. S. Gupta, B. Satpati, P. V. Satyam, B. N. Dev, and D. D. Sarma, J. Phys. Chem. B **108**, 6303 (2004).
[40] F. W. Kleinlein and R. Helbig, Z. Phys. **266**, 201 (1974).
[41] S. G. Gilliland, J. A. Sans, J. F. Sánchez-Royo, G. Almonacid, and A. Segura, Appl. Phys. Lett. **96**, 241902 (2010).
[42] H. Y. Xu, Y. C. Liu, C. S. Xu, Y. X. Liu, C. L. Shao, and R. Mu, J. Chem. Phys. **124**, 074707 (2006).
[43] C. Klingshirn, Phys. Status Solidi B **244**, 3027 (2007).
[44] T. H. Kim, J. J. Park, S. H. Nam, H. S. Park, N. R. Cheong, J. K. Song, and S. M. Park, Appl. Surf. Sci. **255**, 5264 (2009).
[45] J. Dreyhsig and J. W. Allen, J. Phys.: Condens. Matter **1**, 1087 (1989).
[46] F. A. Cotton, D. M. L. Goodgame, and M. Goodgame, J. Am. Chem. Soc. **84**, 167 (1962).
[47] A. B. P. Lever, *Inorganic Electronic Spectroscopy* (Elsevier, Amsterdam, 1984).
[48] R. H. Bube, *Photoconductivity of Solids* (Wiley, New York, 1960).
[49] A. H. Benny and F. D. Morten, Proc. Phys. Soc. **72**, 1007 (1958).
[50] C. A. Johnson, T. C. Kaspar, S. A. Chambers, G. M. Salley, and D. R. Gamelin, Phys. Rev. B **81**, 125206 (2010).
[51] J. Han, P. Q. Mantas, and A. M. R. Senos, J. Eur. Ceram. Soc. **22**, 49 (2002).
[52] F. Bondino, K. B. Garg, E. Magnano, E. Carleschi, M. Heinonen, F. K. Sighal, S. K. Gaur, and F. Parmigiani, J. Phys.: Condens. Matter **20**, 275205 (2008).
[53] S.-H. Wei and A. Zunger, Phys. Rev. B **37**, 8958 (1988).
[54] R. Beaulac, S. T. Ochsenbein, and D. R. Gamelin, in *Nanocrystal Quantum Dots*, edited by V. I. Klimov (Taylor & Francis, New York, 2010).
[55] P. I. Archer, S. A. Santangelo, and D. R. Gamelin, Nano Lett. **7**, 1037 (2007).
[56] K. Ando, H. Saito, Z. Jin, T. Fukumura, M. Kawasaki, Y. Matsumoto, and H. Koinuma, J. Appl. Phys. **89**, 7284 (2001).
[57] C. Klingshirn, R. Hauschild, H. Priller, M. Decker, J. Zeller, and H. Kalt, Superlattices Microstruct. **38**, 209 (2005).
[58] K. Ando, H. Saito, Z. Jin, T. Fukumura, M. Kawasaki, Y. Matsumoto, and H. Koinuma, Appl. Phys. Lett. **78**, 2700 (2001).
[59] W. Pacuski, D. Ferrand, J. Cibert, C. Deparis, J. A. Gaj, P. Kossacki, and C. Morhain, Phys. Rev. B **73**, 035214 (2006).
[60] T. Chanier, F. Virot, and R. Hayn, Phys. Rev. B **79**, 205204 (2009).
[61] R. Beaulac, P. I. Archer, and D. R. Gamelin, J. Solid State Chem. **181**, 1582 (2008).
[62] G. P. Smith, C. H. Liu, and T. R. Griffiths, J. Am. Chem. Soc. **86**, 4796 (1964).
[63] G. Marcotrigiano, L. Menabue, and G. C. Pellacani, J. Coord. Chem. **7**, 1 (1977).
[64] H. A. Weakliem, J. Chem. Phys. **36**, 2117 (1962).
[65] A. Hausmann and H. Huppertz, J. Phys. Chem. Solids **29**, 1369 (1968).
[66] R. S. Title, Phys. Rev. **131**, 2503 (1963).
[67] O. Matumura, J. Phys. Soc. Jpn. **14**, 108 (1959).